2013 LLNL Nuclear Forensics Summer Program

A. B. Kersting

September 27, 2013

Disclaimer

This document was prepared as an account of work sponsored by an agency of the United States government. Neither the United States government nor Lawrence Livermore National Security, LLC, nor any of their employees makes any warranty, expressed or implied, or assumes any legal liability or responsibility for the accuracy, completeness, or usefulness of any information, apparatus, product, or process disclosed, or represents that its use would not infringe privately owned rights. Reference herein to any specific commercial product, process, or service by trade name, trademark, manufacturer, or otherwise does not necessarily constitute or imply its endorsement, recommendation, or favoring by the United States government or Lawrence Livermore National Security, LLC. The views and opinions of authors expressed herein do not necessarily state or reflect those of the United States government or Lawrence Livermore National Security, LLC, and shall not be used for advertising or product endorsement purposes.

2013 LLNL Nuclear Forensics Summer Program

Glenn T. Seaborg Institute
Lawrence Livermore National Laboratory
Physical and Life Sciences
Livermore, CA 94550

Director: Annie Kersting (kersting1@llnl.gov)
Administrator: Camille Vandermeer
Website: https://seaborg.llnl.gov/

Sponsors:
National Technical Nuclear Forensics Center, Domestic
Nuclear Detection Office, Department of Homeland
Security
LLNL: Glenn T. Seaborg Institute, Physical and Life
Sciences Directorate

Disclaimer

This document was prepared as an account of work sponsored by an agency of the United States government. Neither the United States government nor Lawrence Livermore National Security, LLC, nor any of their employees makes any warranty, expressed or implied, or assumes any legal liability or responsibility for the accuracy, completeness, or usefulness of any information, apparatus, product, or process disclosed, or represents that its use would not infringe privately owned rights. Reference herein to any specific commercial product, process, or service by trade name, trademark, manufacturer, or otherwise does not necessarily constitute or imply its endorsement, recommendation, or favoring by the United States government or Lawrence Livermore National Security, LLC. The views and opinions of authors expressed herein do not necessarily state or reflect those of the United States government or Lawrence Livermore National Security, LLC, and shall not be used for advertising or product endorsement purposes.

Auspices

This work was performed under the auspices of the U.S. Department of Energy by Lawrence Livermore National Laboratory under Contract DE-AC52-07NA273

Figure 1.   Annie Kersting, Director, Glenn T. Seaborg Institute (far left), and 2013 Nuclear Forensics Summer Program Students

The Lawrence Livermore National Laboratory (LLNL) Nuclear Forensics Summer Program is designed to give both undergraduate and graduate students an opportunity to come to LLNL for 8–10 weeks for a hands-on research experience. Students conduct research under the supervision of a staff scientist, attend a weekly lecture series, interact with other students, and present their work in poster format at the end of the program. Students also have the opportunity to meet staff scientists one-on-one, participate in LLNL facility tours (e.g., the National Ignition Facility and Center for Accelerator Mass Spectrometry) to gain a better understanding of the multi-disciplinary, on going science at LLNL.

Currently called the Nuclear Forensics Summer Program, this program began 13 years ago as the Actinide Sciences Summer Program. The program is run within the Glenn T. Seaborg Institute in the Physical and Life Sciences Directorate at LLNL. The goal of the Nuclear Forensics Summer Program is to facilitate the training of the next generation of nuclear scientists and engineers to solve critical national security problems in the field of nuclear forensics and have the student experience conducting research at the Lab. We select students who are majoring in physics, chemistry, geology, mathematics, nuclear engineering, chemical engineering and environmental sciences. Students engage in research projects in the disciplines of actinide chemistry, radiochemistry, isotopic analysis, computational analysis, radiation detection, and nuclear engineering in order to strengthen the "pipeline" for future scientific disciplines critical to DHS (DNDO), NNSA.

This is a competitive program with over 80 applicants for the 7–10 slots available. Students come highly recommended from universities all over the country. For example, this year we hosted students from Texas A&M, University of Cincinnati, Washington State University, University of Nevada, Las Vegas, and University of Missouri. (See Table 1).

Lawrence Livermore National Laboratory

This year students conducted research on such diverse topics as actinide (Np, U, Pu) isotopic fingerprinting, statistical modeling in nuclear forensics, actinide analysis for nuclear forensics, environmental radiochemistry, radiation detector materials development, coincidence counting methods, nuclear chemistry, and heavy element separations chemistry (see Table 2.) Graduate students are invited to return for a second year at their mentor's discretion. We encourage the continuation of research collaboration between graduate student, faculty advisor, and Laboratory scientists.

In addition to hands-on training, students attend a weekly lecture series on topics applicable to the field of nuclear forensics (see Table 3). Speakers are experts from both within LLNL and external to it. Speakers are able to discuss the importance of their work in the context of advances in the field of nuclear forensics.

Graduate and undergraduate students on fellowships such as the Nuclear Forensics Graduate Fellowship are invited into our summer program. They usually come for 12 weeks and can return the following summer or stay throughout the year depending on their research needs. This year we had five Nuclear Forensics Fellows, four in the graduate program and one in the undergraduate program (Table 1, noted by an asterisk).

We also host students who are participating in the DOE-sponsored "Summer School in Radiochemistry" course held at San Jose State University and have recruited from this program. They come for a day, meet our summer students, see the research our students are doing, and tour our facilities. Staff scientists also participate in the Nuclear Forensics Undergraduate Summer Program sponsored by DHS-DNDO (FY13 held at University of Nevada, Las Vegas). This year the students come to LLNL for two days to meet our summer students, learn about their research, meet the staff and learn more about work at a national laboratory.

We use our summer program to create a successful pipeline of top-quality students from universities across the U.S. Since 2002, 42 students have returned and/or conducted their graduate research at LLNL:
- 12 became postdoctoral fellows at LLNL.
- 3 became postdoctoral fellows at other national labs.
- 7 were hired as career scientists at LLNL.
- 3 were hired as career scientists at other national labs.
- 3 were hired as faculty in the area of nuclear forensics/radiochemistry/nuclear science.

A big factor in the success of this program is the dedication of the staff scientists who volunteer to mentor the summer students. In FY12, funding from the Nuclear Forensics Graduate Mentoring Program (sponsor: DNDO) helped to partially support the time staff took to teach the summer interns. Staff scientists were able to take the necessary time to develop an appropriate summer project for their student, oversee necessary safety training, and dedicate more time to helping the interns maximize their productivity and scientific potential.

The posters presented at our Laboratory Student Poster Day are included at the end of this report. Two of our students won 'best poster' award out of about 250 poster presentations.
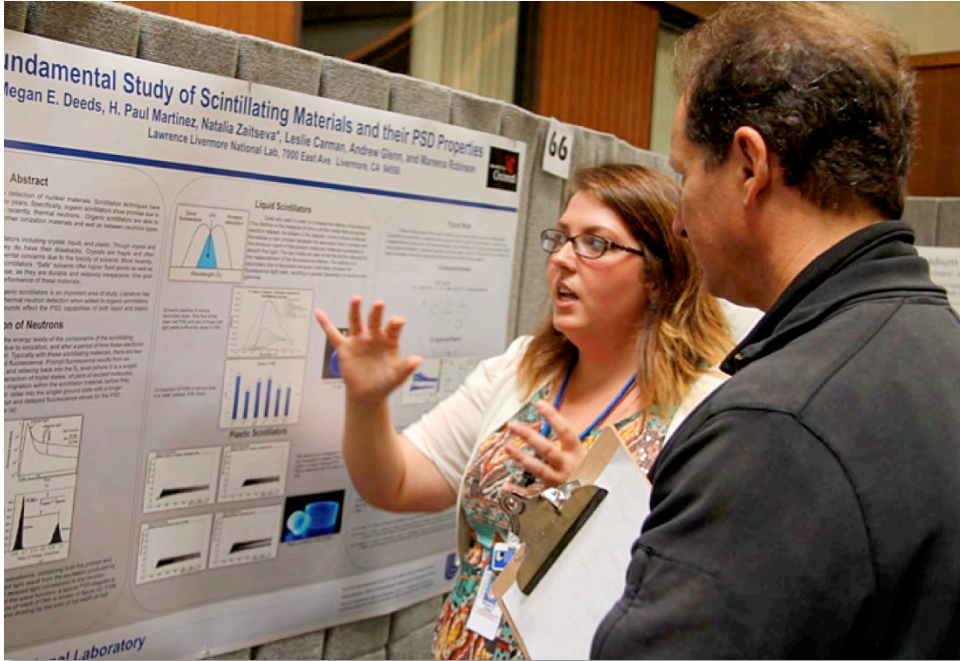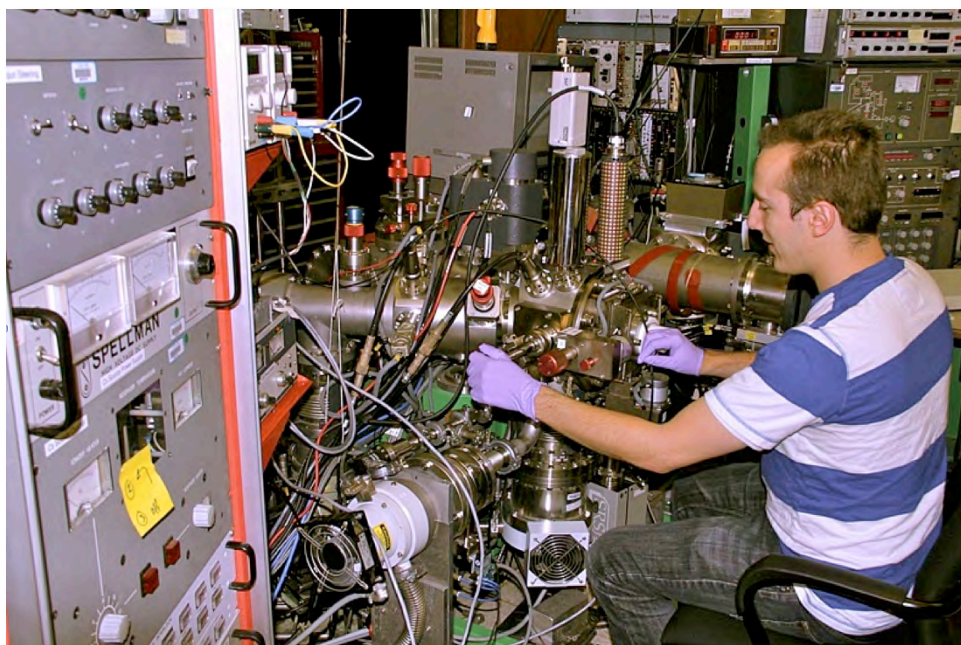
Table 1. **Summer Students**

Student	Major	University	Year
Marisa Alfanso	**Chemistry**	**Texas A&M University, College Station**	**Grad**
Lucas Boron-Brenner	**Radiochemistry**	**University of Nevada, Las Vegas**	**Grad**
Megan Deeds	**Chemistry**	**University of Cincinnati**	**Grad**
Chad Durrant*	**Nuclear Engineering**	**The Pennsylvania State University**	**Grad**
Marc Fitzgerald*	**Chemistry**	**University of Nevada, Las Vegas**	**Grad**
April Gillens*	**Environmental Engineering and Earth Sciences**	**Clemson University**	**Grad**
Mitch Goshert	**Chemistry**	**University of Missouri**	**Grad**
Patrick Harms	**Geology**	**Cal State University, East Bay**	**Grad**
Corey Keith	**Nuclear Engineering**	**Texas A&M University, College Station**	**Grad**
Morgan Kelley	**Radiochemistry**	**Washington State University**	**Grad**
Jeff Rolfes*	**Radiochemistry**	**University of Nevada, Las Vegas**	**Grad**
Rodrigo Tapia**	**Mathematics and Chemistry**	**University of Georgia**	**Undergrad**

*= Nuclear Forensics Graduate Fellows
** = Nuclear Forensics Undergraduate Intern

Lawrence Livermore National Laboratory

Table 2.   Student Projects and Mentors

Student	Mentor	Project
Marisa Alfanso	Dawn Shaughnessy	Analysis of Vanadium Activation Products from NIF Irradiations
Lucas Boron-Brenner	Gary Eppich	U Isotopic Measurements of Fallout Spherules Using Isotope Dilution Mass Spectrometry
Megan Deeds	Natalia Zaitzev	Fundamental Study of Scintillation Materials and their PSD Properties
Chad Durrant*	James Begg/ Mavrik Zavarin	Environmental Transport of Pu: Desorption of Pu in a Multi-Mineral System
Marc Fitzgerald*	Kim Knight	Spatially Resolved Analyses of Historical Fallout
April Gillens*	Mike Singleton	Characterization of TBP using FTIR-ATR and Carbon Stable Isotopes.
Mitch Goshert	Patrick Huang	Bonding and Redox Behavior in Actinide Coordination Complexes: First Principles
Patrick Harms	Brad Esser	Tritium and Stable Isotope Survey of California Surface Water
Corey Keith	Brian Bandong	High Energy Neutron Foil Activation for Davis Cals
Morgan Kelley	Jennifer Jo Ressler	Validation of a Phenomenological Fission Model.
Jeff Rolfes*	Roger Henderson	Development of a Chemical System for Rutherfordium
Rodrigo Tapia**	Brett Isselhardt	Using Computed Tomography to Non-Destructively Characterize Radioactive Fallout in 3D

* = Nuclear Forensics Undergraduate Intern
**= Nuclear Forensics Graduate Fellows

Table 3.   **Seminar Schedule**

Date	Speaker	Topic
6/20/13	**Dawn Shaughnessy** **Group Leader, Experimental Nuclear and Radiochemistry, Chemical Sciences Division**	**Superheavy Element Discovery at LLNL**
6/27/13	**Mona Dreicer** **Deputy Program Director for Nuclear and Domestic Security and Deputy Director of the Center for Global Security Research (CGSR)**	**Treaty Monitoring and Verification**
7/3/13	**Arthur Rodgers** **Scientist, Earth and Energy Division**	**Prompt Forensics with Speed-of-Sound Data**
7/11/13	**Stephan Friedrich** **Scientist, Physics Division**	**Superconducting Gamma Spectrometers with Ultra-high Energy Resolution for Nuclear Forensics**
7/18/13	**James Begg, Postdoc, Chemical Sciences Division** **Greg Brennecka, Postdoc, Chemical Sciences Division**	**Actinides in the Environment** **Geolocation of Nuclear Materials for Forensic Applications**
7/25/13	**Brett Isselhardt,** **Scientist, Chemical Sciences Division**	**Case Studies in Nuclear Forensics**
8/1/13	**Kim Budil** **N Program Manager, Nuclear Counterterrorism, Global Security Principal Directorate**	**A Journey Through the Nuclear Core: A Career at LLNL**
8/8/13	**Annie Kersting** **Director, Glenn T. Seaborg Institute, Physical and Life Sciences Directorate**	**Closing out the program**

Analysis of Vanadium Activation Products from NIF Irradiations

Marisa Alfonso[1,2], Evgeny Tereshatov[1], John Despotopulos[1,3], Narek Gharibyan[1], Ken Moody[1], Dawn Shaughnessy[1]

[1]Lawrence Livermore National Laboratory, Chemical Sciences Division, PLS
[2]Texas A&M University   [3]University of Nevada – Las Vegas

Background

National Ignition Facility (NIF) here at LLNL is a premier nuclear science facility. NIF has the capabilities of producing the world's largest neutron flux - 10^{15} particles. The instantaneous flood of neutrons makes it possible to measure nuclear reaction cross sections without having to correct for late-time neutron contributions, an issue with most other neutron sources. Also, NIF can be used to produce radioisotopes for nuclear forensics exercises.
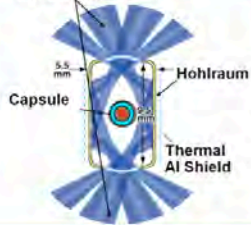
1. Deuterium-tritium fusion creates 14 MeV neutrons
2. Low energy neutrons scatter off the remaining deuterium-tritium and ablator
3. Hohlraum material, mostly gold, is activated and debris is collected
4. Tracer material added to the capsule is activated and collected

To the right is the Diagnostic Insertion Manipulator (DIM) nose cone that position Solid RadioChemistry (SRC) collectors 50 cm from the hohlraum. Two inch diameter ^{nat}V disks (99.75% ^{51}V, 0.25% ^{50}V) were used during these NIF shots. Vanadium metal is frequently used as a SRC collector due to its high melting temperature (1910 °C) and V activation products do not interfere with the gamma detection of the activated gold.

Cross-Section Values From Various Libraries of 14 MeV Neutrons on ^{51}V

	ENDF/B-VI	JENDL-3	JEF-2	CENDL-2	EAF-3	FENDL/A-2	ADL-3T	Average	Std. Dev.	% Std. Dev.
^{51}V(n,α)^{48}Sc	14.9 mb	15.6 mb	19.4 mb	15.31 mb	13.94 mb	14.89 mb	15.42 mb	15.57 mb	1.79 mb	11.5%
^{51}V(n,n-α)^{47}Sc	0.1 mb	0.35 µb	0.19 mb	0.14 µb	2.5 mb	3.84 mb	3.84 mb	0.4 mb	0.93 mb	233 %

^{51}V(n,α)^{48}Sc and ^{51}V(n,n-α)^{47}Sc are two nuclear reactions that occur with ^{nat}V during a NIF shot. As can be seen above there is a large discrepancy in cross section evaluations for ^{51}V(n,n-α)^{47}Sc with 14 MeV nuetrons.[1] After a NIF shot, data from the ^{nat}V collectors can be used to more accurately measure the ^{51}V(n,n-α)^{47}Sc cross section.

Methods
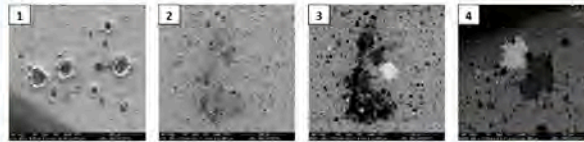
Pictures 1-4 are scanning electron microscope images of a V SRC collector after a NIF shot. The backscattered electron images (3 and 4) show that the collectors are covered in Au and there are spots of Fe (dark) and In (light) hohlraum material.

Picture A shows the V SRC collector after it has been removed from the DIM. To accurately measure the ^{51}V(n,α)^{47}Sc cross section, the V disk needs to be dissolved and the Sc has to be separated from the bulk V material.
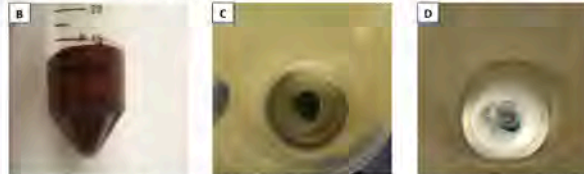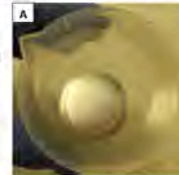
Literature states that V metal dissolves in nitric acid, agua regia, and hot hydrofluoric acid.[2] Many different methods were tested. Passivation occurs (B and C) when using nitric acid or aqua regia to dissolve the V disk. Picture D shows V passivation product being dissolved by concentrated hydrofluoric acid. A mixture of both concentrated nitric and hydrofluoric acid completely dissolves the V disk (E and F). Picture G shows Sc being coprecipitated out of solution as ScF_3 using Ce carrier.[3] The yield of this method is <10% which may be due to formation of soluble complex such as ScF^{-4} and/or the Ce carrier not homogenously mixing throughout the solution.

By adding the carrier to the solution while dissolving the V disk in concentrated nitric acid, the Sc does not get trapped in the passivation product and the carrier is homogenously mixed throughout the solution. Fluoride coprecipitation yield, >70%.

Results
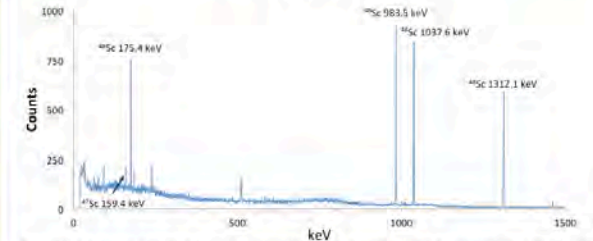
Above is a 3 day spectrum taken at Nuclear Counting Facility of the Sc sample after the V disk was dissolved and Sc was separated from the bulk V material. The precipitate is dissolved using 50/50 (v/v) saturated boric acid and 2 M nitric acid solution. For this sample the ratio of ^{47}Sc/^{48}Sc produced during the NIF shot is 0.0053 ± 0.0006 and the cross section of the ^{51}V(n,n-α)^{47}Sc is calculated* to be 82.8 ± 13.7 µb. A sample from a different shot has a ^{47}Sc/^{48}Sc ratio of 0.007 ± 0.002 and a calculated* ^{51}V(n,n-α)^{47}Sc cross section of 112 ± 33 µb. The two measurements agree within error and have a considerable smaller uncertainty than the evaluated cross section data.[1]

*Assumption made: negligible contribution from ^{50}V(n,α)^{47}Sc and ^{51}V(n,n-α)^{48}Sc cross section equals 15.57 ± 1.79 mb.[1]

Future Work

The assumption made to simplify the ^{51}V(n,n-α)^{47}Sc cross section calculation may not be correct. Assuming that the cross section of the ^{50}V(n,α)^{47}Sc is the same as ^{51}V(n,α)^{48}Sc reaction, the calculated cross section for ^{51}V(n,n-α)^{47}Sc would decrease by 39 µb. A more accurate way to measure both reaction cross section would be to also analysis an enriched V foil after a NIF irradiate. To the left is a foil holder that can be placed behind a SRC collector during future NIF shots. The foil would also have less bulk material, making sample preparation faster and easier.

Acknowledgement

References

1. I.C. Gomes, D.L. Smith and E.T. Cheng, *Status of Cross-Section Data for Gas Production from Vanadium and ^{26}Al from Silicon Carbide in a D-T Fusion Reactor*, 13th Topical Meeting on the Technology of Fusion Energy - 1998 American Nuclear Society Annual Meeting, June 7-11, Nashville, Tennessee (1998).
2. J.L. Brownlee, *The Radiochemistry of Vanadium*, US Atomic Energy Commission Nuclear Science Series NAS-NS 3022 (1960).
3. P.C. Stevenson and W.E. Nervik, *The Radiochemistry of Rare Earths, Scandium, Yttrium, and Actinium*, US Atomic Energy Commission Nuclear Science Series NAS-NS 3020 (1961).

LLNL-POST-641877

URANIUM ISOTOPIC MEASUREMENTS OF FALLOUT SPHERULES USING ISOTOPE DILUTION MASS SPECTROMETRY
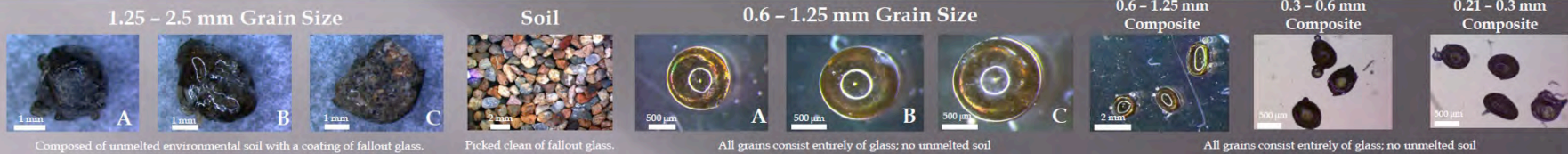
Lucas Boron-Brenner[1], Gary Eppich[2], Kim Knight[2], and Ralf Sudowe[1]

University of Nevada Las Vegas[1], and Lawrence Livermore National Laboratory[2]

Glenn T. Seaborg Institute

UNLV

Goal: To determine uranium concentration and isotopic composition as a function of fallout glass size

1.25 – 2.5 mm Grain Size

Composed of unmelted environmental soil with a coating of fallout glass.

Soil

Picked clean of fallout glass.

0.6 – 1.25 mm Grain Size

All grains consist entirely of glass; no unmelted soil

0.6 – 1.25 mm Composite

All grains consist entirely of glass; no unmelted soil

0.3 – 0.6 mm Composite

0.21 – 0.3 mm Composite

INTRODUCTION

Fallout glass, formed during above-ground nuclear tests, primarily consists of materials incorporated from the nearby environment, (e.g. surface soils) as well as fission and activation products, nuclear fuel that did not undergo fission, and non-nuclear components of the device. The detonation causes the fallout glass to become dispersed into the surrounding area, possibly causing the smallest particles to travel farther from ground zero.

Since the beginning of nuclear testing, little focus has been placed on characterization of test fallout. Analysis of this fallout may provide unique insight into the chemistry and physics underlying nuclear weapons detonations. Data obtained through the chemical and isotopic analysis of fallout will likely be essential in a post-detonation nuclear forensics scenario.

In this study, samples containing fallout were collected from a location proximal to ground zero. Soil and fallout particles were sorted by size, and pieces of glassy fallout were physically separated from the soils from which they were collected. Pieces of fallout were dissolved using mineral acids and analyzed by isotope dilution mass spectrometry (IDMS) to determine fallout uranium concentration and isotopic composition.

Sample Preparation
- Soil separation by grain size using a sieve table.
- Picking of fallout glass assisted by optical microscopy.

Chemical Digestion
- Digestion: 2.5 parts HNO_3 to 1 part HF.
- Addition of $HClO_4$ and 3 M HCl producing stock solution.

Uranium Separation I
- U-TEVA ion exchange with 4 M HNO_3
- Column rinsed using 4 M HNO_3, 9 M HCl, and 5 M HCl.
- Uranium eluted using 0.1 M HCl.

Sample Spiking
- Addition of ^{233}U spike to aliquots of stock solutions, spike equilibration.

Uranium Separation II
- AG1-X8 ion exchange with 9 M HCl.
- Rinsed using 9 M HCl followed by uranium elution using 0.1 M HCl.

Isotopic Analysis
- Analysis performed using MicroMass Isoprobe MC-ICP-MS.

The isotopic composition of individual and composite fallout samples are shown in Panels A and B. These plots demonstrate that the uranium isotopic composition of fallout can be explained through two component mixing between nuclear fuel from the device (approx. 92% ^{235}U) and the natural soil (0.7% ^{235}U). The y-intercept of Panel A represents the $^{234}U/^{238}U$ ratio from the soil end-member. Assuming a device end-member uranium isotopic composition ($^{235}U/^{238}U$ = 92 %), the device $^{234}U/^{235}U$ = 1.09%. When not shown, uncertainty bars are smaller than symbols.

Fallout glass samples (excluding the 0.21-0.3 mm composite) overlap within uncertainty in $^{234}U/^{235}U$ and $^{236}U/^{235}U$, consistent with the two-component mixing model. As in the previous figure, the $^{234}U/^{235}U$ ratio of composite 0.21-0.3 mm is larger. A fraction of glass in the smallest size fraction may have come from a nearby above-ground test, contaminating this size fraction with fallout of a different characteristic $^{234}U/^{235}U$ ratio. The $^{234}U/^{235}U$ and $^{236}U/^{235}U$ ratios measured in these samples may be characteristic of this particular test.

In Panel A, no simple relationship between uranium concentration and $^{235}U/^{238}U$ is observed. The 1.25-2.5 mm samples, which consist of a mixture of unmelted soil and fallout glass, likely vary in U and $^{235}U/^{238}U$ due to their unmelted soil component. The individual 0.6-1.25 mm samples have much higher uranium concentrations than the composite, suggesting that the composites may obscure considerable bead-to-bead heterogeneity in U and $^{235}U/^{238}U$. In Panel B, the 0.21-0.3 mm composite does not overlap within uncertainty relative to most of the other size fractions. This larger ratio suggest an additional uranium component not present in the other size fractions. The source of this additional uranium component may be contamination from another nearby test. Alternatively, the $^{234}U/^{235}U$ ratio may suggest a physical or chemical process occurring during fallout formation not previously identified. When not shown, uncertainty bars are smaller than symbols.

Considerable isotopic variation is observed, both between individual particles, and between particles of different grain sizes. The $^{235}U/^{238}U$ ratio of composite samples decreases with decreasing grain size, suggesting that the smallest fallout glass particles may contain a larger fraction of uranium from soil relative to the device.

ENVIRONMENTAL TRANSPORT OF PU: DESORPTION OF PU(IV) IN A MULTI-MINERAL SYSTEM

Chad Durrant[1,2], James Begg[1], Mavrik Zavarin[1], Pihong Zhao[1], Annie B. Kersting[1]

[1]Glenn T. Seaborg Institute, [2]Penn State University

❶ Plutonium Transport

- Globally ~2000 MT Pu released to the environment [1].
- Understanding subsurface Pu transport is of vital importance.
- Mineral colloids identified as an important transport vehicle for Pu.
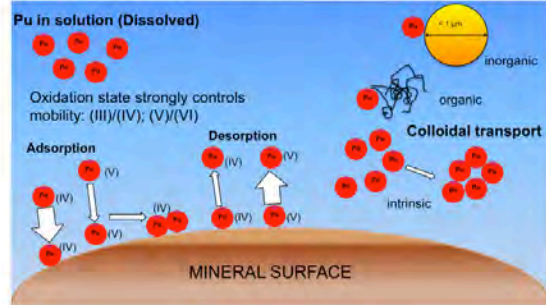- Study Pu-mineral colloid interactions to develop transport models.

Pu in solution (Dissolved)
inorganic
organic
Oxidation state strongly controls mobility: (III)/(IV); (V)/(VI)
Adsorption Desorption Colloidal transport
intrinsic
MINERAL SURFACE

Project Goals

Understanding the behavior of plutonium in complex mineral systems. Specifically, how will adding a second mineral affect the stability of plutonium that is aged onto a first mineral.

❷ Experimental Set-up
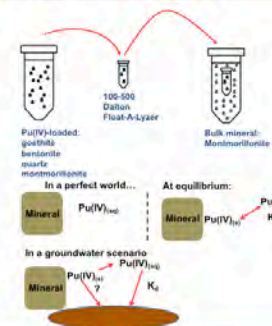
- Studies conducted at pH 4 and pH 8
- Four different minerals
- Aged with Pu(IV)
- [Pu(IV)] is 3×10^{-10} M
- 5 mL of aged sample placed in each Float-A-Lyzer
- The bulk mineral montmorillonite
- [mont] is 5 g/L
- Acts as infinite sink to any plutonium that may desorb

❸ Troubleshooting

Initially no plutonium was seen diffusing through the Float-A-Lyzer membrane. To determine the cause of this phenomena two initial possibilities were raised:

- Perhaps the high concentration of montmorillonite was causing interference during liquid scintillation counting
- Perhaps the pore size was not large enough for Pu to diffuse through
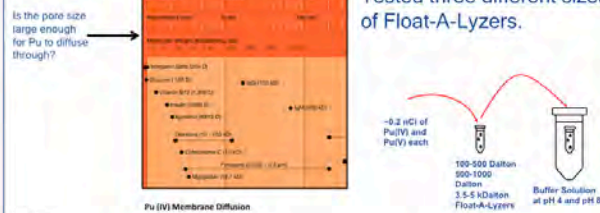
Tested three different sizes of Float-A-Lyzers.

~0.2 nCi of Pu(IV) and Pu(V) each

100-500 Dalton
500-1000 Dalton
3.5-5 KDalton
Float-A-Lyzers

Buffer Solution at pH 4 and pH 8

Pu (IV) Membrane Diffusion

Pu (V) Membrane Diffusion
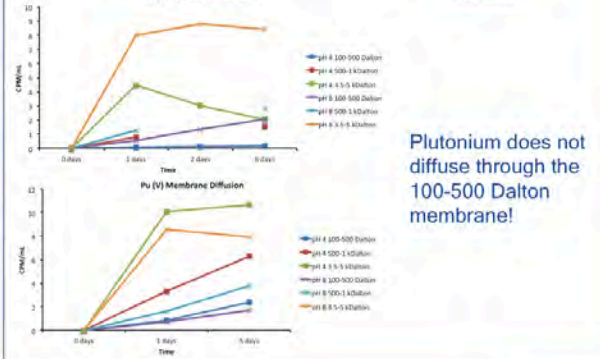
Plutonium does not diffuse through the 100-500 Dalton membrane!

❻ Acknowledgements

1. A. B. Kersting, "Plutonium Transport in the Environment", Inorganic Chemistry, 52 (7), pp. 3533-3546, 2013.

❹ Results

After determining that a larger pore size Float-A-Lyzer was needed the flotation cells were set up again with the remaining goethite and bentonite aged Pu(IV) solutions.

Goethite Cells [Pu] in mol/L
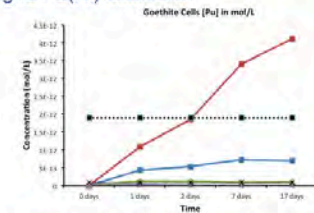
- These two graphs show the ongoing results from the second set of desorption experiments.
- The concentrations represent the amount of plutonium in the bulk phase of the flotation cell.
- The concentration of a 1:1 dilution of the initially free plutonium in the each of the minerals is represented by the dotted line.
- It appears that the addition of a second mineral is increasing the desorption of plutonium from the first mineral in the bentonite cells.

Bentonite Cells [Pu] in mol/L
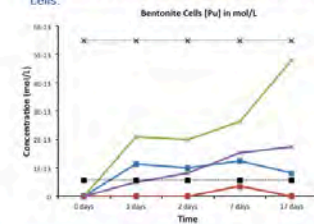
❺ Moving Forwards

Testing the selective affinity for adsorption of plutonium in multiple mineral systems.

Adding organic material to the flotation systems to see the effects on desorption.

Pu

LLNL-POST-

LLNL-POST-761247

Developing Spatially Resolved Analyses of Historical Fallout

Fitzgerald, Marc[1]; Knight, Kim[2]; Stone, Gary[2]; Calderia, Lee[2]; Austin, Kevin[2]; Ramon, Erick[2]; Czerwinski, Ken[1]; Hutcheon, Ian[2]

1. University of Nevada Las Vegas
2. Lawrence Livermore National Laboratory

UNLV

Glenn T. Seaborg Institute

Spatially resolved analyses of fallout can guide our understanding of fallout formation

Overview

Nuclear detonations where fireball ground-contact occurs generate significant quantities of nuclear fallout. This material is created by the vaporization, melting, and scouring action of the fireball on the soil immediately surrounding the device. Since fallout incorporates radioactive traces of the device and event, this material is important for nuclear forensics study. The Trinity device, exploded July 16th, 1945, provides a comparatively well-characterized model system for studying fallout-formation. To understand and characterize this material, we conducted analyses using two methods: autoradiography and microscopy. Microscopy techniques included back-scatter (BSE) and energy dispersive x-ray (EDX) scanning electron microscopy (SEM). These techniques complement each other for the purpose of imaging the spatial deposition of the actinide fuel and/or fission products with respect to major element abundances. **Applying combined spatially resolved measurements, we extracted mixing and formation relationships not accessible through bulk dissolution analysis.**

Theory

Physical basis behind imaging/analytical techniques

SEM-BSE/EDX
- BSE analyses map variations in average Z.
- EDS mapping semi-quantitatively measures major element abundances
- These maps characterize phase relationships in melts

Fig 1a: Electron Beam Interaction Diagram

Autoradiography
- Photostimulable phosphor plates (PSP) are exposed by radiation, producing a latent image
- Latent images are revealed through the digital scanning process
- PSP are not radiation-specific: Alpha and beta cannot be differentiated
- Gamma contribution to image signal is negligible
- Several plates, differing in grain size and emulsion thickness, were investigated for optimization of exposures

Fig 1b: Physics of latent image formation/retrieval in PSP media

Method

Analytical Goals:
- Characterize major element abundance
- Examine spatial dependency of activity
  - Block α to determine β contribution
- Correlate activity and major element compositions through combined imagery

Procedure:
Ten Trinity fallout beads analyzed
- Beads were mounted and polished
- SEM-BSE analysis was performed
- SEM-EDX analytes:
  - Si, Al, Fe, Mg, P, O, Ca, Na, Ti, and K
- Autoradiography
  - 10h56m for alpha/beta
  - 15h 6m for alpha blocked
- ImageJ used for image reconstruction

1.) Sample Mount   2. SEM-(BSE/EDX/WDS)   3. Auto-radiography

Results and Discussion

Fig 2: SEM-BSE and EDX of a single representative spherule. For BSE imaging, areas of lighter intensities correspond to higher atomic number. For EDX maps, areas of lighter intensity correspond to elevated elemental abundance in phases. This sample highlights the extensive contrast between silicon-rich inclusions (sample B, below).

Fig 3: α/β autoradiography shows two distinct modes of spatial activation: surficial and volumetric. The α/β exposure A and C samples demonstrate both extremes (i.e., exclusively surficial or volumetric activation). Exposure B shows some contribution of the two modes. β autoradiography used paper to block α signal to qualitatively confirm that the α/β signal was predominately from α-species (^{239}Pu and ^{241}Am for Trinitite). In most cases, fission products appear to track with alpha species. Despite best efforts, some α-signal had bled through – the basis for this being gamma spectroscopy. Likely beta-emitting isotopes are ^{137}Cs and ^{90}Sr.
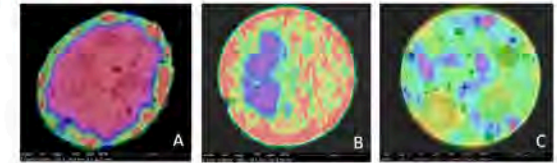
Fig 4: Combined imaging of activity and SEM-BSE analyses reveals the correlation between areas of high activity and high-Z. Warmer colors correspond to areas of higher activity, cooler colors correspond to areas of lower activity. Color scale overlays SEM-BSE images, but is not normalized between spherules.

Examination of corresponding SEM-EDX images (see, for example, Fig 2) show correlations between activity, Ca, Al, Na, K, and Fe. There is an inverse correlation between activity and Si-rich regions. Investigation by EPMA demonstrates that these areas consist of nearly pure silicon dioxide (presumably relict quartz grains), which has a much higher melting point than potassium feldspar (the most likely mineralogical contributor to the CaO-Al_2O_3-SiO_2 rich regions). The preservation of relict quartz would bound maximum heating temperatures of the parent soil to 1700 K. These associations suggest activity dominantly mixed into high abundance, low melting temperature phases. Additionally, activity-iron correlations in most samples suggest iron from the tower tracked the fuel/fission product of the explosion. Alpha and beta activity distributions tend to track one another within samples, contradicting "conventional wisdom" that refractory fuel/fission products are volumetrically distributed and volatile fission products are surficially distributed. (Miller) We hypothesize that observed volumetric and surficial activity distributions are instead a result of solid or partially molten mineral constituents being mixed with molten activity-bearing material. Further investigation and improvements in α/β discrimination is necessary to substantiate this observation.

The Way Forward

Spatially resolved measurements inform formation mechanisms

- Activity-phase correlations would be very difficult or impossible to make using conventional bulk analysis techniques
- We are now developing quantitative high resolution autoradiography to increase the utility of this technique for inter-sample comparisons. See figure 5.
- LA-ICP-MS or SIMS/RIMS based analyses will use the autoradiography information to probe the spatial distribution of actinides and fission products

Fig 5: Silver Halide based autoradiography exhibits higher resolution than PSP autoradiography

References

1.) Handbook of Analytical Methods for Materials. Scanning Electron Microscope.
2.) Physical Electronics Microanalysis Facility. Instrumentation.
3.) Berlin. Nickel High Resolution Beta Imaging. In Handbook of Radioactivity Analysis. 3rd ed. L'Annunziata. Michael F.. Ed.. Academic. Oxford 2012. pp.1208-1240.
4.) Miller, C. F., A Theory of Formation of Fallout from Land-Surface Nuclear Detonations – and Decay of the Fission Products. Technical Report USNRDL-TR-4375. US Naval Radiological Defense Laboratory, 1960.

LLNL-POST-760588

Characterization of TBP using FTIR-ATR and Carbon Stable Isotopes

April R. Gillens[1], Michael Singleton[2], and Brian A. Powell[1]; [1]Environmental Engineering and Earth Sciences, Clemson University, Clemson, SC
[2]Environmental Radiochemistry Group, Chemical Sciences Division, Physical and Life Sciences Directorate, Lawrence Livermore National Laboratory, Livermore, CA

Research Objectives

The objective of this research is to determine the carbon stable isotope signatures of tributyl phosphate (TBP) and its degradation products after contact with nitric acid and sodium hydroxide for the purpose of identifying if there is a unique carbon isotope signature in nuclear reprocessing and solvent disposal. The degradation products considered in this research are limited to dibutyl phosphate (DBP) and butanol. In order to meet this objective, studies will be conducted involving the following instrumentation:

- Fourier Transform Infrared Spectroscopy with Attenuated Total Reflectance (FTIR-ATR)
- Gas chromatography Flame Ionization Detection (GC-FID)
- Gas Chromatography Combustion Isotope Ratio Mass Spectrometry (GC-C-IRMS)

TBP Degradation Mechanisms

Acidic Hydrolysis vs. Basic Hydrolysis

$$(C_4H_9O)_3PO + H_2O \xrightarrow{H^+ + OH^-} (C_4H_9O)_2PO(OH) + C_4H_9OH$$

$$NaOH + CH_3 - CH_2 - CH_2 - CH_2 - O - PO(OC_4H_9)_2$$
$$\xrightarrow{OH^- + Na^+} NaO - P - O(OC_4H_9)_2 + C_4H_9OH$$

Carbon isotope analysis should confirm the degradation mechanisms of TBP in acidic and alkaline conditions. A carbon isotope fractionation is not expected for TBP in alkaline conditions because the P—O bond would rupture keeping the carbon in the molecule intact. A carbon isotope fractionation is expected for TBP in acidic conditions because of the cleavage of the C—O bond associated with TBP degradation under this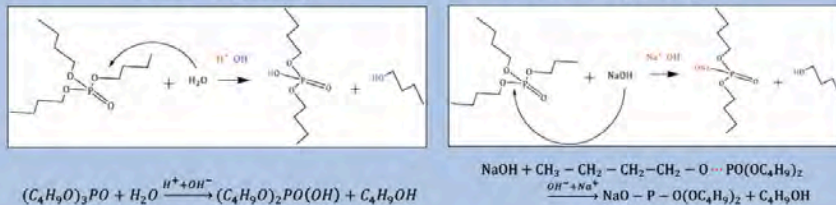 condition. Hence, this work will determine whether there is a unique carbon isotope signature for TBP in nuclear reprocessing and disposal by studying the fundamental characteristics of TBP in acidic and basic hydrolysis. The reaction mechanisms for TBP degradation in acidic and alkaline hydrolysis are distinct. Although the two mechanisms proceed differently, the same degradation products are generated in addition to other products specific to the compound used to degrade the TBP molecule. The majority of degradation products resulting from acidic hydrolysis can be found in both aqueous and organic phases while most of the degradation products from alkaline hydrolysis are found in the aqueous phase. The difference in how TBP degrades in acidic and alkaline media could have major implications on the "signature" of the molecule as a result of its use in nuclear reprocessing and solvent disposal.
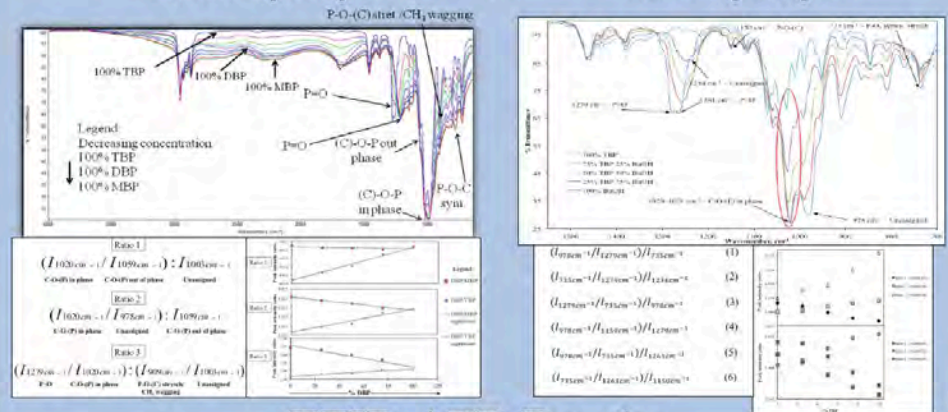
FTIR-ATR Peak Intensity Ratio Technique

Acidic Hydrolysis vs. Basic Hydrolysis

FTIR-ATR Results

A. A sample of TBP degraded in 8 M HNO_3 was evaluated using the peak intensity ratios above. The linear regression developed for a TBP/DBP system saturated in 8 M HNO_3 was used. Ratios 1 and 2 are more reliable and the results of ratio 3 do not reflect the conditions of the sample. After five weeks of hydrolysis, an average of 68% of DBP is produced according to ratios 1 and 2. These results have not be verified by gas chromatography. **B.** This figure describes the average amounts of TBP remaining and butanol formed along with their associated uncertainties for a TBP alkaline hydrolysis experiment involving 12.5 M NaOH, which was characterized by the FTIR-ATR technique using a saturated and unsaturated TBP/butanol system and gas chromatography.

Table 4 Reevaluation of peak intensity ratios of TBP with 8 M HNO_3

Time	Ratio 1 $(I_{1020cm^{-1}}/I_{978cm^{-1}}):I_{1089cm^{-1}}$	% DBP	Ratio 2 $(I_{1020cm^{-1}}/I_{978cm^{-1}}):I_{1123cm^{-1}}$	% DBP
4	0.0121	9.74	0.00785	12.30
12	0.0122	11.24	0.00797	13.81
24	0.0130	20.47	0.00856	21.05
30	0.0131	21.97	0.00866	22.15
36	0.0132	23.27	0.00879	23.76
48	0.0138	29.71	0.00908	27.33
840	0.0167	62.59	0.01287	73.42

Carbon stable isotope signatures of TBP

The GC-C-IRMS system consists of an Agilent 6890 gas chromatograph coupled with a combustion furnace, which leads to an IsoPrime isotope ratio mass spectrometer. The Agilent 6890 gas chromatograph is equipped with a 30 meter by 0.25 millimeter (inner diameter) HP-5MS (5% Phenyl Methyl Siloxane) Ultra Inert fused silica capillary column with 0.25 μm film thickness. Samples are introduced using a splitless/purge injection port set at 250°C. The GC oven is heated using the following program: isothermal for 1 minute at 50°C, 8°C/min to 100°C, 16°C/min to 230°C, 100°C/min to 300°C, and isothermal for 2 minutes for a runtime of 18.08 minutes. Helium is used as carrier gas through the column with a constant flow rate of 0.8 mL/min and average velocity of 32 cm/sec.

Acknowledgements

References

[1] W. W. Schulz and J. D. Navratil, The Science and Technology of Tributyl Phosphate, Vol. 1 CRC Press, Boca Raton, FL (1984).
[2] A. R. Gillens and B.A. Powell, Journal of Radioanalytical and Nuclear Chemistry Vol. 296 No. 2 (2013) 859–868 DOI 10.1007/s10967-012-2147-6

LLNL-POST-637732

Bonding and Redox Behavior in Actinide Coordination Complexes: A First Principle Study

Mitchell Goshert,[1] Patrick Huang,[2] and Justin Walensky[1]
Physical and Life Sciences Directorate and Glenn T. Seaborg Institute
[1]University of Missouri, Columbia
[2]Lawrence Livermore National Laboratory

INTRODUCTION – REDOX POTENTIAL

- Aqueous uranyl and plutonyl dinitrates are common by-products of nuclear fuel reprocessing.
- What is their long-term mobility and fate?
- Oxidation state determines solubility and consequently the mobility in the environment.
- What are the thermodynamic parameters characterizing the transformation between oxidation states?
- Actinides in solution exhibit a large variation in oxidation state and coordination number.
- Contributions due to variations in actinide speciation difficult to disentangle experimentally.
- Calculations of reduction potential can provide useful insight on the energy required to reduce these actinide species.

THEORETICAL METHODOLOGY

Hartree-Fock (HF)

$$\left[-\frac{\hbar^2}{2m} \nabla_i^2 + V_i^{eff}(\mathbf{r}_i) \right] \varphi_i(\mathbf{r}_i) = \varepsilon_i \varphi_i(\mathbf{r}_i)$$

- Mean field approximation: Each electron feels the same averaged, effective potential due to the remaining electrons.
- Does not include electron-electron correlation → qualitative, but not quantitatively accurate.
- Useful as starting point for higher-level theories.

Density Functional Theory (DFT)

- Mean-field theory (like Hartree-Fock).
- Approximate inclusion of electron correlation via model exchange-correlation functional v_{xc}.
- We employ the B3LYP approximation for v_{xc}:
  1. Generally improves bond energies and lengths over HF.
  2. Better-suited for localized d- or f-electrons (minimizes self-interaction error).

SOLVENT MODEL

Conductor-like Polarizable Continuum Model (CPCM)

- Solvent effects are an important influence on reduction potentials.
- Model solvent as a continuum dielectric.
- Need to assume a conductor-like cavity containing solute.
- CPCM well-established for polar solvents (e.g., water).

Shape-adapted cavity   Spherical cavity

- For large, unspherical complexes, shape-adapted cavities are necessary.

CALCULATION OF REDUCTION POTENTIALS

- Free energies are calculated relative to a standard hydrogen electrode.

$$An^{VI} + e^- \rightarrow An^V$$
$$\tfrac{1}{2}H_2 + H_2O \rightarrow H_3O^+ + e^-$$
$$An^{VI} + \tfrac{1}{2}H_2 + H_2O \rightarrow An^V + H_3O^+$$

OPTIMIZATION OF BOTH U(VI) AND U(V) SPECIES

- The structures of the $UO_2(NO_3)_2(H_2O)_2$ complex in both U(VI) and U(V) oxidation states were optimized.
- Vibrational analysis was employed to verify the stability of optimized structures.

- The optimized structures of U(VI) (left) and U(V) (right).

STRUCTURES

$U^{VI}O_2(NO_3)_2(H_2O)_2$ – Bond Lengths

	HF (gas)	HF (solv)	B3LYP (gas)	B3LYP (solv)	Expt.
U=O [Å]	1.71	1.71	1.77	1.77	1.76
U-O$_{H2O}$ [Å]	2.56	2.53	2.55	2.52	2.45
U-O$_{NO3}$ [Å]	2.50	2.53	2.49	2.50	2.48

*Experimental data from Dalley, N.K.; Mueller, M.H.; Simonsen, S.H. Inorg. Chem. 1971, 10, 323.

- B3LYP shows an improved U=O bond length over HF to within ~ 0.01 Å.
- Both HF and B3LYP yield significant lengthening of both U-O$_{H2O}$ bonds relative to experiment.
- Both HF and B3LYP accurately predict the U-O$_{NO3}$ bond length within ~0.02 Å.

$U^{V}O_2(NO_3)_2(H_2O)_2$ – Bond Lengths

	HF (gas)	HF (solv)	B3LYP (gas)	B3LYP (solv)	Expt.
U=O [Å]	1.80	1.81	1.84	1.85	-
U-O$_{H2O}$ [Å]	2.73	2.63	2.71	2.62	-
U-O$_{NO3}$ [Å]	2.67	2.63	2.61	2.61	-

- Uranyl V bond lengths show ~0.1 Å increase on average over uranyl VI.

REDUCTION POTENTIALS

	E^0 (gas) HF	E^0 (solv) HF	E^0 (gas) DFT	E^0 (solv) DFT
$U(VI) + e^- \rightarrow U(V)$	2.12	4.22	2.86	4.60
$\tfrac{1}{2}H_2 + H_2O \rightarrow H_3O^+ + e^-$	-8.02	-4.67	-8.96	-5.78
Reduction Potentials	-5.90	-0.45	-6.10	-1.18

- Inclusion of solvation effects yields a ~ 4.9 eV improvement over the gas phase model.
- Discrepancy between E^0 (solv) and expt. likely due to:
  1. Errors in H_2 half-reaction.
  2. Lack of explicit second coordination sphere.
- Errors for calculated actinide reduction potential typically ~ 2-3 eV
  [Hay, J. P.; Martin, R. L.; Schreckenbach, G. J. Phys. Chem. A 2000, 104]
- Experimental data for the reduction potential of $UO_2(H_2O)_5$ is 0.16 eV, meaning our data is reasonable.
  [Brand, J. R.; Cobble, J. W. Inorg. Chem. 1970, 9, 912.]

CONCLUSIONS – REDOX POTENTIALS

- Benchmark studies have been done on $UO_2(NO_3)_2(H_2O)_2$ VI and V
- Our model involves an explicit representation of the first coordination sphere plus a continuum dielectric for the solvent environment.
- Solvation effects are essential for description of red. potentials.

INTRODUCTION – BONDING BEHAVIOR

- Uranium trioxide, UO_3, is the major precursor used for nuclear energy throughout the world.
- However, due to its poor solubility in organic solvents, little chemical information is known about UO_3.
- Examining the structure, bonding, and reactivity of analogs will provide insight into UO_3 chemistry.
- The Bart group at Purdue University has synthesized two tris(imido)uranium complexes which are isoelectronic with UO_3.
- Ab Initio methods were used to calculate the ground state structure of the synthesized compounds.

STRUCTURES – GEOMETRY OPTIMIZATION

- Geometry optimizations were performed on both the U(PDI)(NDIPP)$_3$ (left) and U(PDI)(NMes)$_3$ (right)

PDI = pyridine (diimine)
DIPP = 2,6 = diisopropylphenyl
Mes = 2,4,6 = trimethylphenyl

	Exp.	Comp.	Exp.	Comp.
U-N$_{PDI(left)}$ [Å]	2.609	2.621	2.552	2.581
U-N$_{PDI(center)}$ [Å]	2.587	2.584	2.580	2.566
U-N$_{PDI(right)}$ [Å]	2.609	2.641	2.553	2.578
U-N$_{imido(axial)}$ [Å]	1.966	2.014	1.995	2.009
U-N$_{imido(eq.)}$ [Å]	2.021	2.032	2.024	2.030
U-N$_{imido(axial)}$ [Å]	1.965	2.017	1.992	2.010

CONCLUSIONS – BONDING BEHAVIOR

- A successful geometry optimization has been completed on the U(PDI)(NDIPP)$_3$ complex with bond lengths within ~0.05 Å accuracy
- The U(PDI)(NMes)$_3$ optimization has not fully converged but demonstrates an accuracy within ~0.03 Å.

ACKNOWLEDGEMENTS

LLNL-POST-641750

Tritium and Stable Isotope Survey of California Surface Water

Patrick A. Harms[1], Jean E. Moran[1], Ate Visser[2], Brad K. Esser[2]

[1]California State University, East Bay, Department of Earth and Environmental Sciences
[2]Chemical Sciences Division, Glenn T. Seaborg Institute, Lawrence Livermore National Laboratory
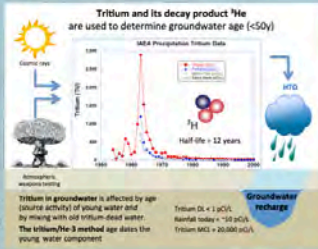
Abstract

The purpose of this study is to characterize the isotopic signature of precipitation in California watersheds. Measurements of tritium, ^{2}H and ^{18}O from surface water are used as a proxy to identify regional isotopic features.

Introduction

Tritium (^{3}H) and the stable isotopes of water (^{2}H and ^{18}O) are used to examine watershed dynamics, identify water provenance and determine water residence times. These isotopes are extremely useful as a natural tracer because they follow the path of water as part of the water molecule. Stable isotopes in precipitation have a strong spatial signal that indicates the source of the water. Tritium, which is produced cosmogenically in the upper atmosphere, has a strong temporal signal that allows for age dating of water. Large quantities of ^{3}H were created by atmospheric thermonuclear weapon testing between 1953-1963. Current tritium concentrations in precipitation are approaching pre-nuclear levels.

The strong topographic gradient in California (Pacific Ocean to Sierra Nevada) results in distinct tritium and stable isotope signatures, making these tracers especially useful in water resources and age dating investigations.

Tritium and its decay product ^{3}He are used to determine groundwater age (<50y)

Tritium in groundwater is affected by age (source activity) of young water and by mixing with old tritium-dead water.

The tritium/He-3 method dates the young water component.

Tritium DL < 1 pCi/L
Rainfall today < ~10 pCi/L
Tritium MCL = 20,000 pCi/L

Methods

Field
- Over 40 surface water locations visited across California
- Tritium (^{3}H) and stable isotope (^{2}H and ^{18}O) samples collected in non-preserved 1L and 30 ml glass bottles respectively.
- Water quality parameters recorded with YSI 556.

Lab

Tritium measurements by ^{3}He accumulation (LLNL)
- ^{3}H samples degassed under vacuum to remove decay-product ^{3}He.
- ^{3}He accumulated for at least 21 days.
- ^{3}He cryogenically separated and measured by mass spectrometry.

Stable Isotopes (CSUEB)
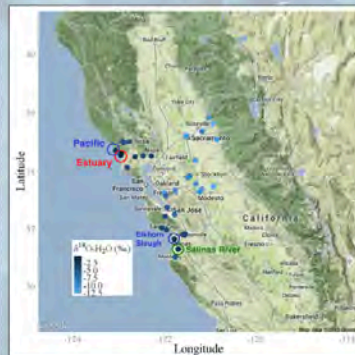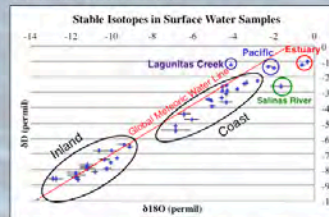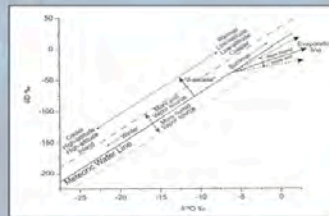- ^{2}H and ^{18}O measured by cavity ring-down laser absorption spectrometer.

In the field, sampling and recording water quality parameters.

Samples hanging on manifold for degassing under vacuum.

Samples kept frozen with dry ice after cryogenic separation of ^{3}He gas from water.

Results
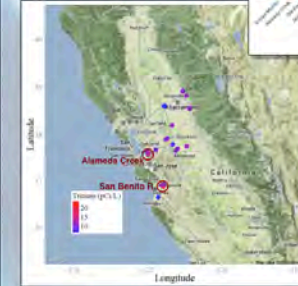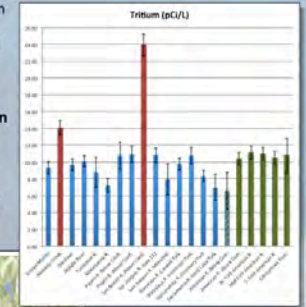
Stable Isotopes

- δD and δ^{18}O are expressed as $\delta(\text{in permil}) = [(R_{sample}/R_{standard})-1]*1000$, where R is ratio of heavy to light isotopes.
- **The Global Meteoric Water Line (GMWL)** represents empirical relationship between δD and δ^{18}O found in meteoric water.

- **Pacific Ocean** sample (blue circle) is similar to **Vienna Standard Mean Ocean Water** (VSMOW: δD=0 and δ^{18}O=0).
- **Elkhorn Slough** (also in blue circle) is similar to Pacific due to **ocean influence**.
- **Estuary** samples (red circle) show **evaporation effects**: heavier (less negative) δ^{18}O and δD than source water (Pacific Ocean). This effect is stronger for hydrogen than oxygen.
- **Coastal samples** are **lighter** than ocean water due to preferential evaporation of light isotopes.
- **Salinas River** sample (green circle) also shows **evaporation effects** with coastal water as source.
- **Inland samples** are **lighter** than coastal samples due to rainout of heavy isotopes.
- **Lagunitas Creek** (purple circle) and some inland samples show **deuterium excess** from re-evaporation and precipitation of terrestrial water.

GMWL and factors that affect isotopic ratios of deuterium and oxygen (McGuire and McDonnell, 2006).

Stable Isotopes in Surface Water Samples

Map of δ^{18}O in sampled surface water. Strong west to east gradient visible due to rainout of heavier isotopes near coast.

Map of surface water samples with deuterium excess. Most d-excess occurs inland, with the exception of Lagunitas Creek.

Tritium

- **High** concentration of tritium found in **Alameda Creek** and **San Benito River** (red bars).
- Tritium concentration generally **higher** with **less variability** at high elevation rivers (green bars).
- Tritium concentration **significantly lower** below **Folsom Lake** (striped bar), showing effects of reservoir on tritium decay.

Tritium (pCi/L)

Discussion and Future Work

Discussion
- Preliminary tritium data shows possible elevation gradient and reservoir effects.
- Stable isotope results are consistent with the known coastal to inland and low to high elevation gradients
- Evaporation effects are also apparent from δD and δ^{18}O offset from the GMWL.

Future Work
- **Spring sampling** - Surface waters will be resampled during the spring runoff period when precipitation signal will be stronger.
- **More watersheds** - Future sampling will include watersheds farther to the north and south as well as the Sierras.
- **Continue tritium analysis** – Because of 21 day accumulation period, not all samples were analyzed in time to be included with these results.
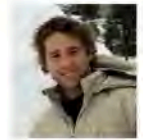
LLNL-POST-641739

High-Energy Neutron Foil Activation for Davis Cals

Corey Keith[1], Bryan Bandong[2], Robert Haslett[2], Kip Harward[2], Tzu Wang[2], Kevin Roberts[2]

[1]Texas A&M University, Department of Nuclear Engineering, College Station, TX
[2]Lawrence Livermore National Laboratory, Physical and Life Sciences, Chemical Sciences Division, Livermore CA

Davis Cals are inter-laboratory measurements and calibration comparisons of "threshold detector products". High-energy neutron foil activation is used for the isotope production, and the goal is to model this process and compare to experimental results.

Introduction

Radioanalytical measurements on activation species are being performed by LLNL, LANL, and PNNL. The activation species used for the inter-laboratory measurements are produced at the 76-inch Cyclotron at UC Davis Crocker Nuclear Laboratory by irradiating various detector metal foils with high-energy neutrons produced from bombarding a thick beryllium target with 40 MeV deuterons. The existing nuclear data for (d,n) reactions for beryllium, as well as production cross sections for the foils, are very limited in the evaluated energy ranges of the fast neutron spectrum. As a result, it was proposed to use physics models and Monte Carlo codes to simulate isotope production and compare with recent experimental results.

Neutron Flux Profile on Au Foil

To evaluate the differences between physics models and beam width on isotope production, the neutron flux profile on Au foil was evaluated.
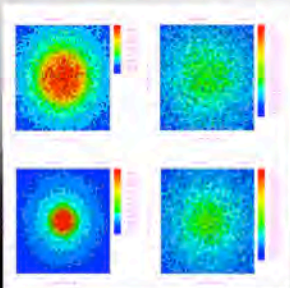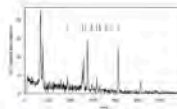

Top Left: INCL4 0.5 cm beam width; Bottom Left: INCL4 0.25 cm beam width; Top Right: Bertini 0.5 cm beam width; Bottom Right: Bertini 0.25 cm beam width

Setup

Various physics models that use both intranuclear cascade (INC) and evaporation physics were used to model (d,n) reactions. Early results showed that, for 40-MeV deuterons, changes in evaporation models had little impact, and so differences between three INC models (CEM03[1], Bertini[2] and INCL4[3]) were evaluated. MCNPX 2.7 was used to evaluate neutron transport in the system and reaction rates in the foils.
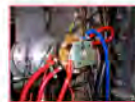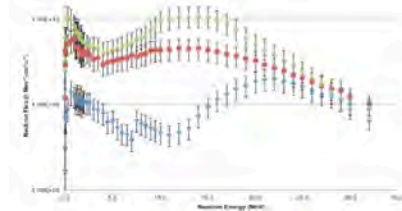

*Top: Picture of Beryllium Target and foil assembly
Bottom: MCNP modeled geometry
Right: Gold foil Gamma Spectrum[4]*

Isotope Production

Isotope Production for the gold and titanium foils were evaluated using MCNPX and the ENDF and TENDL cross sections. The activation run was conducted on 12/27/2012

Neutron Flux

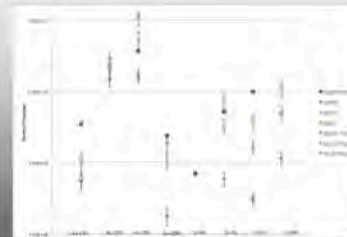Neutron Flux for various INC physics models evaluated for a for a 6.0 ± 1.7 μA beam current.

Discussion

The three INC models all have limits of reliability in the energy range being explored when compared with recent experimental data. The TENDL cross sections for higher energy are in good agreement for the [195]Au, [196]Au, [46]Sc, [48]Sc residual cross sections. Further work is needed to asses production pathways and cross sections for [44]Sc, [47]Sc, and [194]Au.

References:

1. S.G. Mashnik, et al., LANL Report LA-UR-05-7321, Los Alamos, 2005, RSICC Code Package PSR-532.
2. H.W. Bertini Phys. Rev., 131 (1963), p. 1801
3. A. Boudard et al. Phys. Rev. C. 66 (2002), p. 044615
4. J. J. Wilkens, Activation of Implanted Gold At. Proton Beams, NPTC (2004) 01

NUCLEAR ENGINEERING TEXAS A&M UNIVERSITY

Validation of a Phenomenological Fission Model WASHINGTON STATE UNIVERSITY

Morgan Kelley[1], Walid Younes[2], Jennifer Jo Ressler[2]

[1]Washington State University, Department of Chemistry, Pullman, WA

[2]Lawrence Livermore National Laboratory, Physical and Life Sciences, Nuclear Physics Division, Livermore CA

Fission data are very useful for both forensic and basic science applications. Unfortunately, these data often cannot be easily measured experimentally. Therefore, fission models/theories play an important role to fill in the gaps left by experiment. We will determine the extent to which the fission model GEF can be trusted.

GEF: GEneral Fission model

GEF[1] uses Monte Carlo methods used to calculate:
- Element & isotope yield distribution, before and after neutron emission
- Mass chain yields
- Isomer yields
- Angular momentum distribution
- Prompt gamma and neutron spectra
- Total kinetic energy of fragments
- Numerous other fission observables

Uncertainties are determined based on perturbed parameters during iterative calculations.

First Assessment: GEF vs. Experiment

Due to larger experimental uncertainties, the Pu239 Thermal data and GEF data match fairly well, while the U235 Thermal data from experiment is often outside of the GEF values.
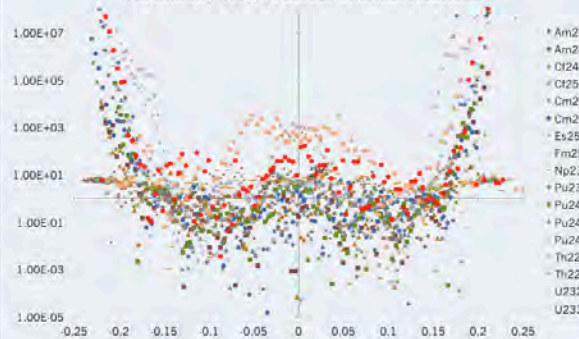

U235 – Thermal Neutrons

Pu239 - Thermal Neutrons
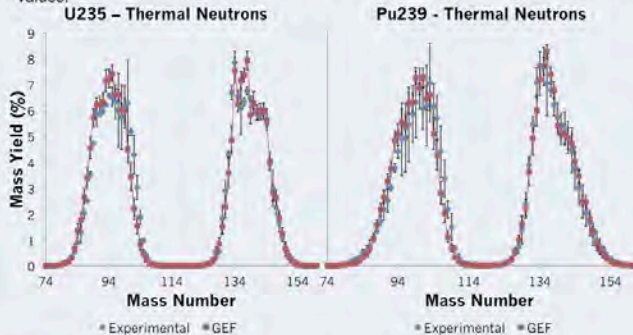
To treat the data in a more rigorous way, χ^2 for each fission product mass was calculated for various nuclides, and compared to the asymmetry:

$$Asymmetry = (Mass(Fragment) - 1/2\ Mass(Nuclide))\dagger2\ /Mass(Fragment)\dagger2$$

$$\chi\dagger2 = [Yield(Exp) - Yield(GEF)]\dagger2\ /Uncertainty(Exp)\dagger2$$

Asymmetry vs. χ Squared: Thermal Neutrons

A single χ^2 value was then calculated for each nuclide and compared to the 95% critical value, testing if an obvious reason to reject the model existed. For low-yield masses, GEF's calculated yields are eclipsed by their uncertainties. To exclude these values from the χ^2 calculation, a yield threshold was set and systematically tested. These χ^2 values were calculated taking correlation into account:

$$\chi\dagger2 = \Delta Y\dagger T \times V\dagger -1 \times \Delta Y$$

ΔY is a vector containing the difference between experimental and GEF yields for each mass, and v is the covariance matrix of the calculated GEF yields.
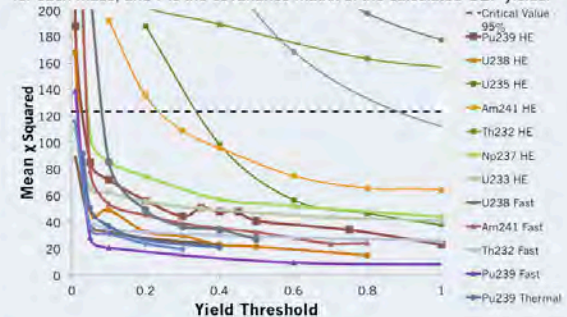

Mass-Chain Yields

In most cases, GEF does an acceptable job of reproducing experimental yields. However, for particular nuclides, the GEF calculations match experimental data mostly thanks to the large uncertainties that GEF calculates.
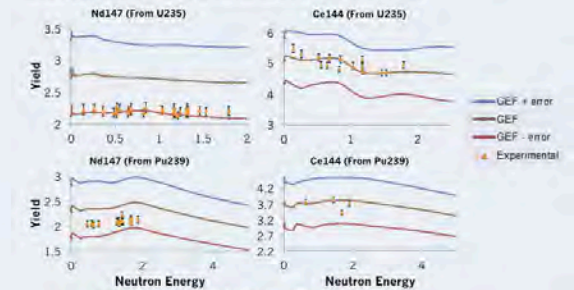
Uncertainty Analysis

χ^2 values for most nuclides are well below the 95% confidence limit (GEF may be overestimating uncertainties). Edited the GEF code to include an error factor: a factor by which the internal GEF parameters – the parameters perturbed to generate the calculated uncertainty – are multiplied by. Investigated the effects of varying the error factor. Attempted to decrease the uncertainty without causing χ^2 to increase to the 95% critical value. In all cases except U235 thermal, the uncertainty calculated by GEF can be reduced.
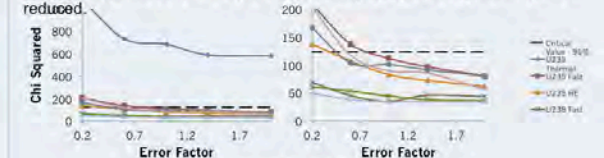
Conclusions

1. For many nuclides, GEF does an acceptable job of reproducing experimental values within experimental error.
2. GEF gives a good starting point for an estimate of experimental yields. However, the type of validation presented here is critical to properly use these estimates and their respective uncertainties.
3. As a phenomenological model, GEF is useful to more fundamental approaches because it helps us understand many important features of fission.

1. K.-H. Schmidt and B. Jurado, JEF/DOC 1423 (2011). GEF code and documentation available for download at http://www.cenbg.in2p3.fr/-GEF

LLNL-POST-641741

Development of a Chemical System for Rutherfordium

Jeff Rolfes[1], John Despotopulos[1,2], Roger Henderson[2], Ralf Sudowe[1]

[1]University of Nevada, Las Vegas
[2]Lawrence Livermore National Laboratory

Background

Studies of the chemical properties of the heaviest elements have always been difficult due to the short half-lives and low cross sections involved. To solve this problem, atom-at-a-time methods are used to determine the properties of short-lived isotopes. Extremely fast kinetics for the chemical reactions studied (on the same order as the nuclide's half-life) are required and the system should have potential for automation. One potential technique, extraction chromatography, offers a way of investigating rutherfordium's properties, without the solvent waste generated in liquid-liquid extractions.

A fast systematic method involving the use of a ligand with higher inner group selectivity is necessary to discover more about element 104. Using the homologs, zirconium and hafnium, studies can be performed using liquid-liquid extractions and extraction chromatography. From literature reviews, thiacrown ethers, tertiary amines, and calixarenes show promise in extracting group 4 elements. The development of an extraction system for rutherfordium based on these extractants can further elaborate on its properties.

40
Zr

72
Hf

104
Rf
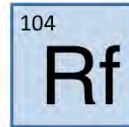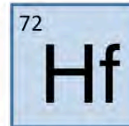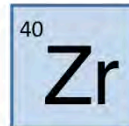
Purpose

While the primary goal of research involving rutherfordium and its homologs is to study superheavy element chemistry, this research and techniques can be directly applied to zirconium separations in post-detonation material as zirconium is a major fission product. The speed of separations required for superheavy element chemistry is on the order of seconds. SCUREF's *Technical Mission Area 1* specially mentions speed accuracy and precision concerning the analysis of nuclear materials.
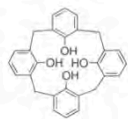
The surrounding ligands will be all tested, beginning with TEHA. All of them have shown promise in the extraction of zirconium and hafnium in literature, but have not been fully examined for their usefulness in fast chemistry.
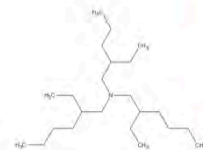
Tris-2-ethylhexyl amine (TEHA)

Dicyclohexano-18-crown-6

Calix[4]arene

Calix[6]arene

Thiahexa-18-crown-6

Procedure

To initially examine the ligand for its suitability for superheavy element chemistry, a solvent extraction is first performed on the suspected homologs of the element of interest. An aqueous phase of varying acid concentrations is prepared and added to an organic phase with the dissolved ligand.

A spike of a radioactive tracer (either ^{89}Zr, ^{95}Zr, or ^{175}Hf) is then added to the phases.
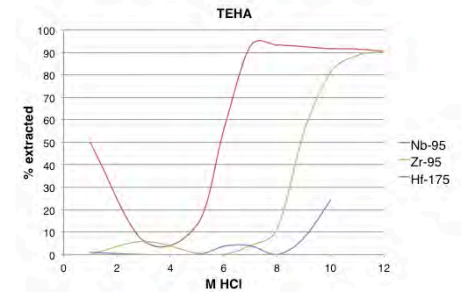
The spiked phases then are mixed vigorously on a shaker for 30 minutes.
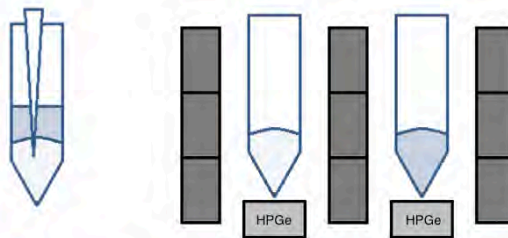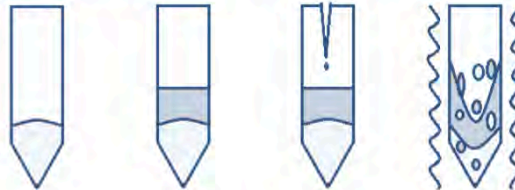
HPGe

HPGe

After equilibrium has been reached, the aqueous and organic phases are separated into different vials.

The phases are currently counted on a HPGe detector due to the interference of the ^{95}Nb peak being 10 keV away from the ^{95}Zr peak. In the future, samples will be counted on an automated NaI detector using a ^{68}Zr tracer.

Physical and Life Sciences Directorate

Preliminary Results

TEHA

- Nb-95
- Zr-95
- Hf-175

(% extracted vs. M HCl)

Preliminary data shows a marked separation of zirconium and hafnium. Niobium's extraction is also included as well since it is a decay product of ^{95}Zr. It is important to note that the ^{95}Zr used has stable carrier added to it, so its results cannot be directly correlated to the chemical behavior of single atoms due to the amount of Zr polynuclear species formed.

Goals

For the rutherfordium work, the new ligands mentioned will be tested using ^{89}Zr, ^{95}Zr, and ^{175}Hf by performing solvent extractions with hydrochloric acid. In addition, the dicyclo-18-crown-6 will tested with nitric and sulfuric systems.

If the kinetics are fast, then synthesizing a resin for extraction chromatography and conducting batch studies will be the next step. If any of these extraction system appears show promise, then it will be tested at Texas A&M's cyclotron using short-lived isotopes of zirconium and hafnium. Finally, it will be applied to the study of rutherfordium.

Acknowledgements

References

1) R. Sudowe, *et al. R. Acta. 94* (2006) 123–9
2) R. Banda, *et al. J Rad Nucl Chem.* (2013) 13-18
3) R. Wolf , *et al. Inorg. Synth.* **25** (1989) 123-6
IM: LLNL-POST-641875

Using Computed Tomography to Non-Destructively Characterize Radioactive Fallout in 3D

Lawrence Livermore National Laboratory

Glenn T. Seaborg Institute

The University of Georgia

Rodrigo N. Tapia, B. H. Isselhardt, K. B. Knight, J. D. Sain, I. D. Hutcheon

Goal: Develop method to analyze 3D density distributions of fallout provided by computed tomography (CT). In particular, exploring the correlation of X-ray attenuation with average electron density.

Overview:

This project is divided into two main objectives: the exploration of compositional analysis by density mapping and the quantification of void spaces within fallout spheres using CT. Fallout glasses are the resulting debris formed from the rapid vaporization and condensation of ground and device materials during a nuclear detonation.
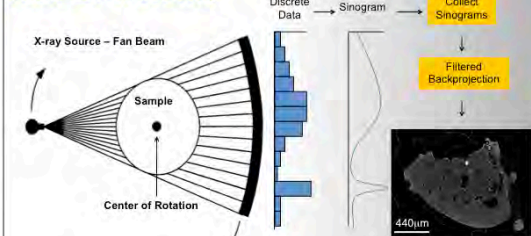
Why: Void Analysis
- Rapid heating and cooling causes vesicles
- Vesicles are formed by gases that do not fully evolve
- Statistical distributions can help describe timeframe of formation

Why: Density Mapping
- CT provides a 3D density map related to X-ray attenuation
- Greater attenuation is displayed as higher intensity
- X-ray attenuation is correlated to average electron density
- Average electron density is a function of density and atomic number
- This correlation has potential to identify compositions of interest

How CT it Works

Discrete Data → Sinogram → Collect Sinograms → Filtered Backprojection

X-ray Source – Fan Beam
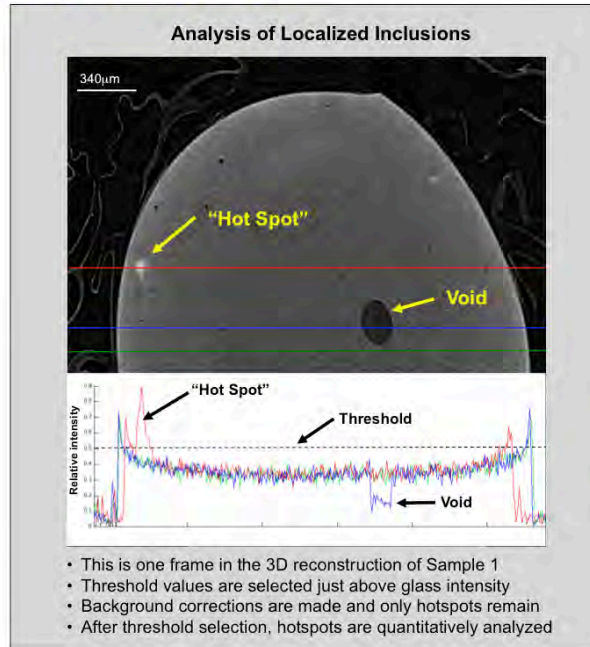Sample
Center of Rotation

Rotating sample is irradiated by Bremsstrahlung X-ray source. The transmitted X-rays are detected on a CCD array at 360° rotation. Internal structure is reconstructed based on X-ray attenuation at various angles.

Sample mounting
13 mm
13 mm

3D Image Data
- Maximum X-ray energy ranged 70-80kV
- Reconstructed data provides images with associated 3D units
- Voxels are the 3D analog for pixels
- Pixel dimension ranged 1.178-2.661μm
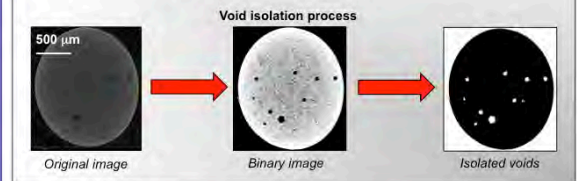- Field of view ~5mm

Results: Density Analysis

Analysis of Localized Inclusions

340μm
"Hot Spot"
Void

"Hot Spot"
Threshold
Void
Relative intensity

- This is one frame in the 3D reconstruction of Sample 1
- Threshold values are selected just above glass intensity
- Background corrections are made and only hotspots remain
- After threshold selection, hotspots are quantitatively analyzed

Localized Hotspots of High Attenuation

	Material	Mean Intensity	Linear Attenuation Coefficient Normalized to Glass
Sample 1	Glass	0.4079	N/A
	Hotspot 1A	0.8094	0.6853
	Cold Spot	0.3335	-0.2014
Sample 3	Glass	0.3670	N/A
	Hotspot 3A	1.6739	1.5175
	Hotspot 3B	2.3276	1.8472
	Hotspot 3C	2.7638	2.0190

Sample 3: Hotspot 3B
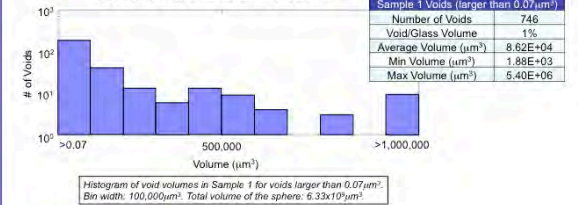440μm

False color CT image of fallout glass
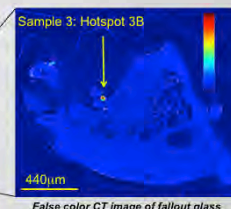
Results: Void Analysis

Developed void isolation algorithm:
1. Isolated volumes of low attenuation
2. Reduced noise and established thresholds to identify voids
3. Calculated void volume and statistics

Void isolation process

500 μm
Original image → Binary image → Isolated voids

Volume Distribution of Voids

# of Voids
Volume (μm³)
>0.07   500,000   >1,000,000

Sample 1 Voids (larger than 0.07μm³)	
Number of Voids	746
Void/Glass Volume	1%
Average Volume (μm³)	8.62E+04
Min Volume (μm³)	1.88E+03
Max Volume (μm³)	5.40E+06

Histogram of void volumes in Sample 1 for voids larger than 0.07μm³. Bin width: 100,000μm³. Total volume of the sphere: 6.33x10⁹μm³.

Conclusions:

- We can spatially resolve objects on the order of 10 microns
- Average electron density and X-ray attenuation are correlated
- We can locate high density inclusions in fallout
- Beam hardening does not significantly impact relative intensity
- Distributions of voids may inform time-temperature sample history

Future Steps:

- Compute 3D maps of fallout features
- Perform CT analyses on 5 additional fallout samples
- Analyze a set of 4 standard metals with CT (Ta, Co, In, Al)
    - Construct a calibration for density vs. attenuation
- Study the relationship between attenuation and composition in fallout
- Analyze hotspots by scanning electron microscopy

Acknowledgements: